

High Throughput Methodology for Synthesis, Screening, and Optimization of Solid State Lithium Ion Electrolytes

Mark S. Beal,[†] Brian E. Hayden,^{*,†} Thierry Le Gall,[†] Christopher E. Lee,[†] Xiaojuan Lu,[†] Mehdi Mirsaneh,[†] Claire Mormiche,[†] Denis Pasero,[†] Duncan C. A. Smith,[†] Andrew Weld,[†] Chihiro Yada,[‡] and Shoji Yokoishi[‡]

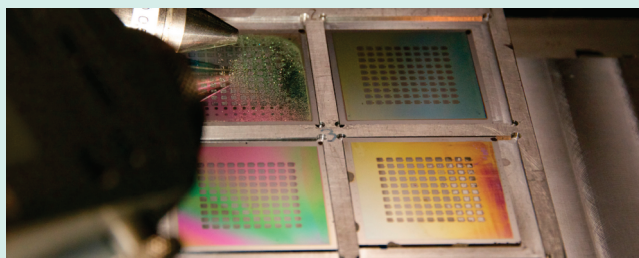
[†]Ilika Technologies, Kenneth Dibben House, Enterprise Road, University of Southampton Science Park, Southampton, SO16 7NS, U.K.

[‡]Toyota Motor Corporation, Battery Research Division, Higashifuji Technical Centre, 1200 Mishuku, Susono, Shizuoka, 410-1193, Japan

S Supporting Information

ABSTRACT: A study of the lithium ion conductor $\text{Li}_{3x}\text{La}_{2/3-x}\text{TiO}_3$ solid solution and the surrounding composition space was carried out using a high throughput physical vapor deposition system. An optimum total ionic conductivity value of $5.45 \times 10^{-4} \text{ S cm}^{-1}$ was obtained for the composition $\text{Li}_{0.17}\text{La}_{0.29}\text{Ti}_{0.54}$ ($\text{Li}_{3x}\text{La}_{2/3-x}\text{TiO}_3$ $x = 0.11$). This optimum value was calculated using an artificial neural network model based on the empirical data. Due to the large scale of the data set produced and the complexity of synthesis, informatics tools were required to analyze the data. Partition analysis was carried out to determine the synthetic parameters of importance and their threshold values. Multivariate curve resolution and principal component analysis were applied to the diffraction data set. This analysis enabled the construction of phase distribution diagrams, illustrating both the phases obtained and the compositional zones in which they occur. The synthetic technique presented has significant advantages over other thin film and bulk methodologies, in terms of both the compositional range covered and the nature of the materials produced.

KEYWORDS: solid state electrolyte, thin film, neural network



INTRODUCTION

The advancement of solid state battery technology is dependent on the development of highly conductive, stable electrolytes. A rapid means to explore candidate electrolyte materials is therefore of great interest. We present here a high throughput methodology for the synthesis, characterization, and optimization of thin film, solid state lithium ion electrolyte materials. The perovskite $\text{Li}_{0.34}\text{La}_{0.51}\text{TiO}_{2.94}$ ($\text{Li}_{3x}\text{La}_{2/3-x}\text{TiO}_3$ $x = 0.11$) has previously been reported to have a bulk conductivity of $10^{-3} \text{ S cm}^{-1}$ and a total conductivity of $7 \times 10^{-5} \text{ S cm}^{-1}$.¹ Further work demonstrated that the bulk lithium ion conductivity varies along the $\text{Li}_{3x}\text{La}_{2/3-x}\text{TiO}_3$ ($\sim 0.15 > x > \sim 0.04$) solid solution line, with an optimum value at $x = 0.1$.² Kawai and Kuwano also reported that at the upper limit of lithium content ($x > \sim 0.15$) $\text{Li}_{1.33}\text{Ti}_{1.67}\text{O}_4$ and $\text{Li}_2\text{La}_2\text{Ti}_3\text{O}_{10}$ crystalline phases were observed in addition to the solid solution. Materials produced at the lower limit of lithium content ($x \sim 0.04$) were observed to give rise to a mixture of $\text{La}_2\text{Ti}_2\text{O}_7$ and the perovskite phase. Generally this system is produced by traditional sintering methods, as in the previous examples; however, thin films have been produced by a number of routes including: sol-gel,³ laser ablation,^{4–6} and e-beam evaporation.⁷ As a result of the extensive work published in the literature and the high lithium ion conductivities previously measured, this system is an ideal benchmark for a high throughput screen.

A successful solid state electrolyte material must demonstrate a high ionic conductivity, although this may be compromised by utilizing a thin film ($< 1 \mu\text{m}$). In addition to being a selective ion conductor (to prevent material breakdown), the material should have a very low electrical conductivity ($< 10^{-12} \text{ S cm}^{-1}$) to ensure a long operating lifetime.⁸

The high throughput physical vapor deposition system (HT-PVD), described previously,^{9,10} provides a means to produce thin film sample libraries, containing hundreds of compositionally unique fields. This synthetic method has been previously used by the authors for studies of metallic alloys,¹¹ Au nanoparticles on substoichiometric oxides,¹² hydrides,¹³ and complex oxides.¹⁴

A complete comparison of this synthetic method with other high throughput thin film techniques is beyond the scope of this report; however, it is possible to set this method in the context of other thin film methods. There are broadly two groups of thin film synthesis: “fast sequential” and parallel. The former is characterized by the use of user defined masks or moving shutters to build up layers of different elements resulting in a net variation in composition.^{15–18} Typically this is followed by heating, to achieve efficient mixing of the different layers;¹⁹ however,

Received: November 29, 2010

Revised: April 7, 2011

Published: April 11, 2011

efficient mixing has been achieved by depositing sequential sub-atomic layers of various elements.^{19,20} The latter parallel approach takes advantage of the natural profile of off-axis sources which, under the right conditions, give deposition rates which vary across the sample. By controlling the relative rates of the elements this method has been shown to yield control over compositional ranges.^{21,22}

The parallel HT-PVD method is simple, since shadow masks are only needed if discrete samples are required. Additionally, depositions can typically be accomplished in one layer, because the elements are deposited simultaneously; therefore, the process can be accomplished quickly and without the need for thermal treatment. Combining this synthetic method with fast sequential screening of electrical properties, structural and elemental compositions, it is possible to rapidly accelerate the rate of materials development. These experimental techniques yield large data sets, which are not readily analyzed by hand. Therefore chemometric techniques such as principal component analysis (PCA); multivariate curve resolution-alternating least-squares (MCR), and artificial neural networks (ANN) have enabled the elucidation of optimum material and synthetic parameters within this system. These show good agreement with the existing literature.¹ In addition, data mining techniques have been applied to determine the synthetic parameters which contribute to producing properties, such as a capacitive response or higher purity perovskite materials.

EXPERIMENTAL PROCEDURES

Synthetic Methodology. The HT-PVD system comprises a physical vapor deposition (PVD) chamber with a plurality of interchangeable off-axis electron beam evaporator or Knudsen cell sources, for co-evaporation of elemental Li, La, and Ti onto a substrate in the presence of atomic oxygen, produced from a plasma source. Each source is independently controlled in terms of both the thickness gradient (“wedge”) across the substrate and the rate of deposition. The wedge is obtained by placing a shutter in a predetermined position prior to commencing the deposition process. This creates a shadow on the substrate. Compositional gradients can thereby be controlled utilizing both the source temperatures and the wedge positions, a distinct advantage compared to other natural profile deposition techniques. The synthetic system is described in detail elsewhere.^{9,10}

Experimental Section. Depositions were carried out on a range of substrates including: MgO; multilayer substrates; Si/SiO₂/Ti/Pt (SSTP); Si/SiO₂/TiO₂/Pt (SSTOP); Si/SiO₂/TiO₂/Pt/SrRuO₃ (SSTOP/SRO); sputtered SrRuO₃ on Si (Si/SRO) and Silica/Pt. Lithium was heated in an effusion source; titanium and lanthanum were heated in electron beam evaporators. Molecular oxygen was dissociated using a plasma source. This was situated such that a direct line of sight existed between the sample and the source. Deposition times varied between 20 and 180 min. Complete synthetic details can be found in the Supporting Information.

The elemental compositions (Li, La, Ti atomic percentage) of the sample libraries were measured utilizing Laser Ablation Inductively Coupled Plasma Mass Spectroscopy. This method allows the quantification of light elements such as lithium, which would not be possible with methods such as Energy Dispersive Spectroscopy.

Thickness measurements were made using a spectroscopic ellipsometer. Spectroscopic impedance measurements were made via an array of 0.25 mm platinum contacts which were sputtered onto

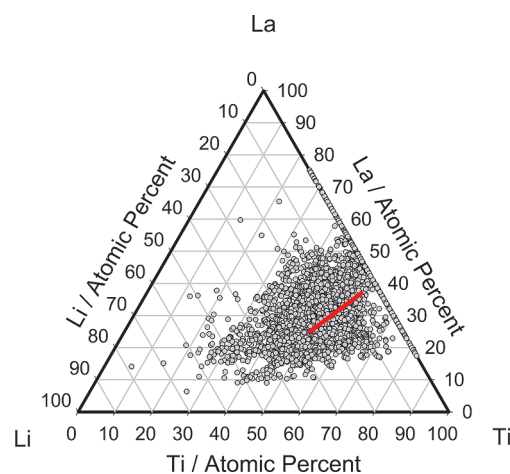


Figure 1. Distribution of data set across composition space. The $\text{Li}_{3x}\text{La}_{2/3-x}\text{TiO}_3$ solid solution line is shown in red for observed perovskite materials.²³

the sample libraries. These measurements were automated using a probe station. X-ray diffraction measurements were carried out on the sample libraries as close as possible to the electrode arrays. Diffraction data is generally reported for the range $20.8 \leq 2\theta \leq 36.78^\circ$ to avoid the dominant Pt (100) reflection at $39.76^\circ 2\theta$ from the underlying substrate. Throughout, measurements were made on every field within the sample library providing a consistent data set.

Description of Samples and Analysis Methods. Thirty five sample libraries were synthesized, on five different substrates. The focus of the synthetic work was the $\text{Li}_{3x}\text{La}_{2/3-x}\text{TiO}_3$ solid solution line, encompassing the region surrounding this line. This line and the distribution of the compositional data around the line are shown in Figure 1. The thickness of the fields within these libraries varied between 76 and 972 nm

All sample libraries synthesized at 25°C were amorphous prior to ex situ thermal treatment. Crystalline materials were observed when samples were deposited at elevated temperature and following annealing. Diffraction data from representative samples of the composition $\text{Li}_{0.17-0.18}\text{La}_{0.26-0.27}\text{Ti}_{0.55-0.56}$, deposited on SSTOP, are shown in Figure 2. The field deposited at 25°C was observed to be amorphous. Diffraction peaks were observed in the fields annealed to 700°C and deposited at 700°C . Following thermal treatment, the samples exhibited defects such as pinholes or cracking. Macro scale decrepitation was also observed in certain regions of sample libraries.

Within the frequency limitations of the impedance instrumentation used throughout this investigation, it was not possible to observe the characteristic “blocking spike”, typical of bulk oxide lithium ion conductors at room temperature.^{6,24} It was also not possible to distinguish bulk and grain boundary components of the impedance response. This observation has been previously reported.^{4,6} Since we are unable to distinguish bulk from grain boundary conductivities, *all conductivity values reported here refer to total ionic conductivity.*

In addition to capacitive behavior, we also observed mixed and electrically conductive materials. This was attributed to the multiphase nature of the thin films, which may include electrically conductive phases such as TiO_{2-x} . Traditional analysis, suitable for bulk samples, concentrates on the complex plane (Cole–Cole plot) which emphasizes the most resistive elements in the

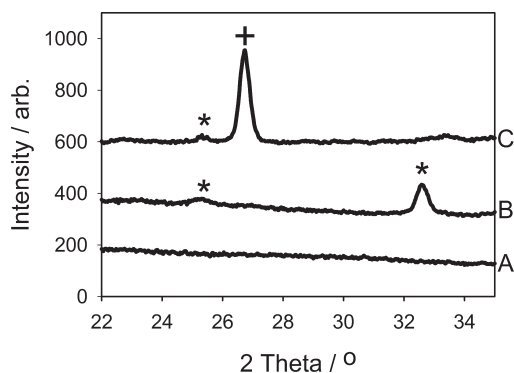


Figure 2. X-ray diffraction measurements of $\text{Li}_{0.18}\text{La}_{0.27}\text{Ti}_{0.55}$ oxide thin film as deposited at 25 °C on SSTOP (A), $\text{Li}_{0.17}\text{La}_{0.27}\text{Ti}_{0.56}$ oxide deposited at room temperature and annealed at 700 °C in O_2 (B), $\text{Li}_{0.18}\text{La}_{0.26}\text{Ti}_{0.56}$ oxide deposited at 700 °C (C). X-ray diffraction data is shown for the region of interest $20.8^\circ \leq 2\theta \leq 36.78^\circ$. The peaks marked * are attributed to the tetragonal $\text{Li}_{3x}\text{La}_{2/3-x}\text{TiO}_3$ $x = 0.17$. The peak marked + is assigned to $\text{La}_4\text{Ti}_9\text{O}_{24}$.

measured sample. To highlight the components with the smallest capacitance it is necessary to determine the maxima in the Modulus plot (M'' vs f).^{24,25}

To process the raw electrochemical impedance data into a useful figure of merit for our investigation, it was initially necessary to classify the data into one of four responses. The classification of materials as “straight short”, “resistive short”, “mixed conductor”, and “capacitive” was determined by the different types of response observed within a given frequency range ($1 - 10^6$ Hz). Data which did not fall into one of the four categories above was classified as “insulating”. For typical samples, these criteria can be evaluated as thresholds, detailed in the Supporting Information with examples of data.

Once classified, the total ionic conductivity of the material was calculated. The method used was specific to the behavior observed. The conductivity of materials exhibiting straight shorts was calculated by determining the material resistance using the Z'' value at the minimum Z'' value. In the case of resistive shorts, the conductivity was calculated by finding the maximum value in the M'' versus $\log f$ plot.^{24,25} Assuming a single resistor and capacitor in parallel, the conductivity of the material was then determined using eq 1. In the case of both mixed conductors and capacitive behavior the resistance of the material is determined using the modulus method.^{24,25} Gaussian curves were fitted to the M'' versus $\log f$ plot to determine both the maximum modulus value and the frequency at which it occurs. The resistance of the material was then determined using eq 1. Materials exhibiting behavior which could not be classified by any of the criteria detailed above, or gave rise to Gaussian curve with poor fits, were classified as resistive. Analysis of the whole data set, including raw data sets (XRD and electrochemical impedance), was carried out using MATLAB (2010a, The Mathworks), including the PLS_Toolbox (5.5.1, EigenVector Research) and JMP (8, SAS).

$$\sigma = \frac{d\pi f_{\max}}{AM''_{\max}} \quad (1)$$

Where d is the thickness of film/m, f_{\max} is the frequency of observed maximum in M'' versus frequency plot/Hz, A is the area of contact/ m^2 , and M''_{\max} is the maximum value of M'' observed in the M'' versus frequency plot.

RESULTS AND DISCUSSION

To establish an overview of the large data set (6276 fields) it was beneficial to use a summary plot, such as that generated using recursive partitioning. In this case, a decision tree was produced showing the number of fields exhibiting a given impedance behavior. The splitting of the data within the analysis was carried out by searching all possible divisions and selecting the division which maximized the significance of each split. Analyzing the data using such a recursive partition method, we observed that 19.0% of the samples deposited on SSTOP, Silica/Pt, and SSTOP/SRO (Group A) exhibited capacitive behavior. Within the second group of substrates SSTP, Si/SRO and MgO/Pt, (Group B) 1.4% of the samples exhibited such behavior. In this instance, analysis was limited to the synthetic parameters (substrate, thermal processing temperatures) and elemental composition (see Supporting Information). Note that the distribution of compositions within Group A and B were similar (see Supporting Information) assuring us that the difference observed because of the substrates is not confounded with the composition.

Phase Behavior of Samples Deposited on SSTOP. In an effort to further understand the crystallization behavior of this system, 18 sample libraries, all deposited on SSTOP were selected for further analysis. In this case, the diffraction data, in addition to the electrical response, was analyzed. The diffraction data was factorized into components using multivariate curve resolution-alternating least-squares (MCR).^{26,27} The concept of this process is shown in eq 2: m samples with n intensity measurements make up the data matrix, the resultant analysis presents the scores and loadings of i components. In all MCR models reported here, closure constraints and non-negative constraints were applied.

$$\{\text{Data Matrix}(m \times n)\} =$$

$$\{\text{Model scores}(m \times i)\} \times \{\text{Model loadings}(i \times n)\} + \text{Error} \quad (2)$$

The scores were interpreted as a series of fractional concentrations for each of the i identified components. The loading data was interpreted as diffraction patterns for each of the i identified components. A complete explanation of this methodology is given by Long et al.²⁶ Since this analysis does not take into account the structure factor for each of the different phases, the percentage values shown here can only be taken as a first approximation of the true values.

The number of components required to describe the diffraction data sufficiently, was determined by comparing the variance captured using a Principal Component Analysis (PCA) model and that captured by the MCR model.²⁶ Thirteen components were selected to model the SSTOP data set.

Once calculated, the component patterns of the model were compared to literature diffraction patterns (ICDD database, PDF 4+, 2009). The thirteen components were attributed to six unique materials. Multiple components were attributed to $\text{La}_4\text{Ti}_9\text{O}_{24}$, $\text{La}_2\text{Ti}_2\text{O}_7$, and TiO_{2-x} ($x = 0.25, 0.33$). It is thought that multiple components were required to describe these single phases, because of different degrees of preferential orientation across multiple sample libraries. The resultant changes in peak intensities, because of orientation, lead to the identification of multiple components for a single phase. In the case of TiO_{2-x} distinct patterns were expected as a result of differing oxygen stoichiometries.

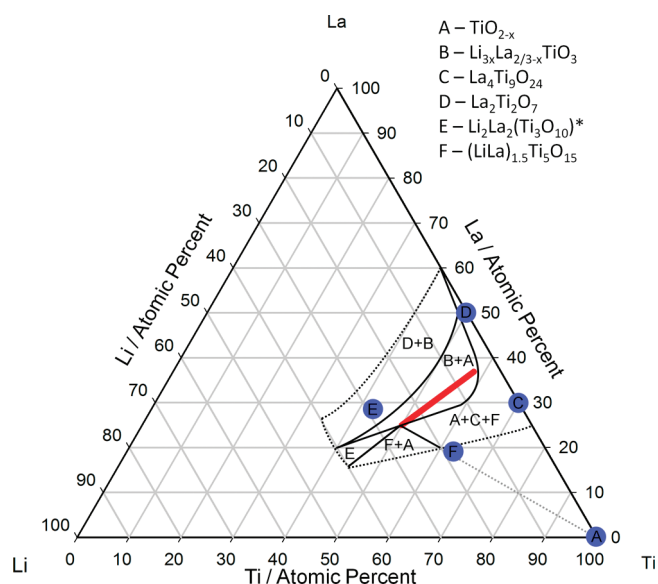


Figure 3. Crystalline phase distribution map for samples deposited on SSTOP at 25 °C and annealed at 700 °C in O₂. The bold solid red line indicates the position of the known Li_{3x}La_{2/3-x}TiO₃ solid solution line.²³ The positions of the pure phases observed are shown in blue. Solid black lines indicate the boundaries between mixed phases, as determined from mean distribution of components. The dashed black lines indicate the extent on the data set. The gray line indicates the predicted extension of the TiO_{2-x} + La₄Ti₉O₂₄ + (LiLa)_{1.5}Ti₅O₁₅ region. The asterisk above the Li₂La₂(Ti₃O₁₀) phase indicates that this is the parent compound; the phase identified within the MCR model is thought to be a modified form of this material.

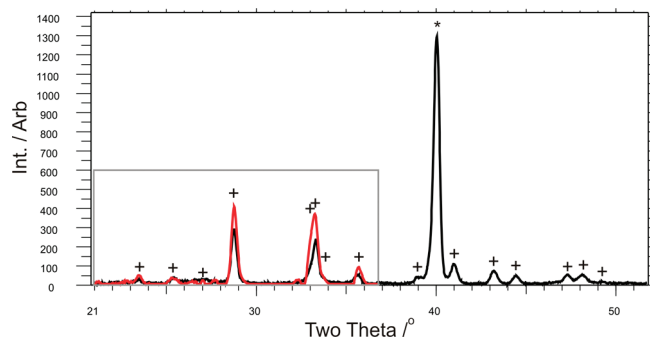


Figure 4. Baseline corrected diffraction pattern of Li_{0.30}La_{0.22}Ti_{0.48} deposited on SSTOP at 25 °C and annealed in O₂ for 3 h at 700 °C (black). This material was calculated to have a Li₂La₂(Ti₃O₁₀) (01-087-1169) component score (concentration) of 0.83. The region of the diffractogram analyzed using MCR is highlighted in gray (20.8° ≤ 2θ ≤ 36.78°). The peak positions of Li₂La₂(Ti₃O₁₀), with a reduced *c*-axis, are indicated by the + signs. The peak marked * is attributed to the Pt(100) reflection.

From this analysis it was possible to illustrate the distribution of phases across compositional space, Figure 3. Although the phase distributions encompass the position of the pure phases (with the exception of Li₂La₂(Ti₃O₁₀)) the distributions do not exactly match those expected at thermodynamic equilibrium. This diagram should not be considered as an equilibrium phase diagram, but instead as a crystalline phase distribution map observed within these thin films, as a function of composition.

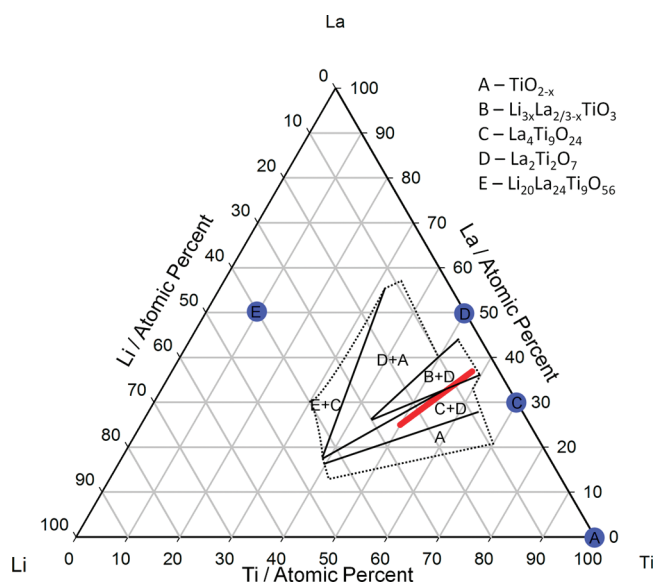


Figure 5. Crystalline phase distribution map for samples deposited on MgO at 700 °C. The bold solid red line indicates the position of the known Li_{3x}La_{2/3-x}TiO₃ solid solution line. The positions of the pure phases observed are shown in blue. Solid black lines indicate the boundaries between mixed phases, as determined from mean distribution of components. The dashed black lines indicate the extent on the data set.

In the case of Li₂La₂(Ti₃O₁₀) the crystalline phase distribution map indicated a region away from the pure phase composition of this phase (Figure 3). Examination of the MCR component reveals that this component can be attributed to the Li₂La₂(Ti₃O₁₀) material, with a reduced *c*-axis (26.4383 Å cf. 26.56 Å, 0.45% reduction). This reduction is concomitant with the increased lithium concentration within the material. A material with a high component score (0.83) for this phase is shown in Figure 4. The calculated pattern for the Li₂La₂(Ti₃O₁₀) with a reduced unit cell is also shown. Previous work by Kawai and Kuwano has shown that a small amount of Li₂La₂(Ti₃O₁₀) is obtained in bulk samples when excess lithium is used to prepare the Li_{3x}La_{2/3-x}TiO₃ solid solution.²

Phase Behavior of Samples Deposited on MgO/Pt. In the same manner as described previously, four samples deposited on MgO, were analyzed using the PCA and MCR method. In this case six components were noted to describe the data adequately. The six components were compared to a database of diffraction patterns and were assigned to five phases: La₄Ti₉O₂₄, Li₂₀La₂₄Ti₉O₅₆, La₂Ti₂O₇, TiO_{2-x} (*x* = 0.14) and Li_{3x}La_{2/3-x}TiO₃ (*x* = 0.11). Two components were attributed to the La₂Ti₂O₇ phase. It was noted that the modified Li₂La₂(Ti₃O₁₀) phase observed previously was not observed in this system, instead the same compositional region is occupied by a mixture of La₄Ti₉O₂₄ and TiO_{2-x}, Figure 5. Because of the low diffraction cross section of Li, crystalline materials dominated by this element may be missed in thin film materials.

Synthesis of Crystalline Li_{3x}La_{2/3-x}TiO₃. Performing recursive partitioning analysis on the calculated percentage of crystalline Li_{3x}La_{2/3-x}TiO₃ within the 3903 fields deposited on SSTOP allowed us to determine the important factors in achieving high concentrations of crystalline Li_{3x}La_{2/3-x}TiO₃. Figure 6 illustrates that the primary difference in the data was determined to be caused by the concentration of lithium within the thin film.

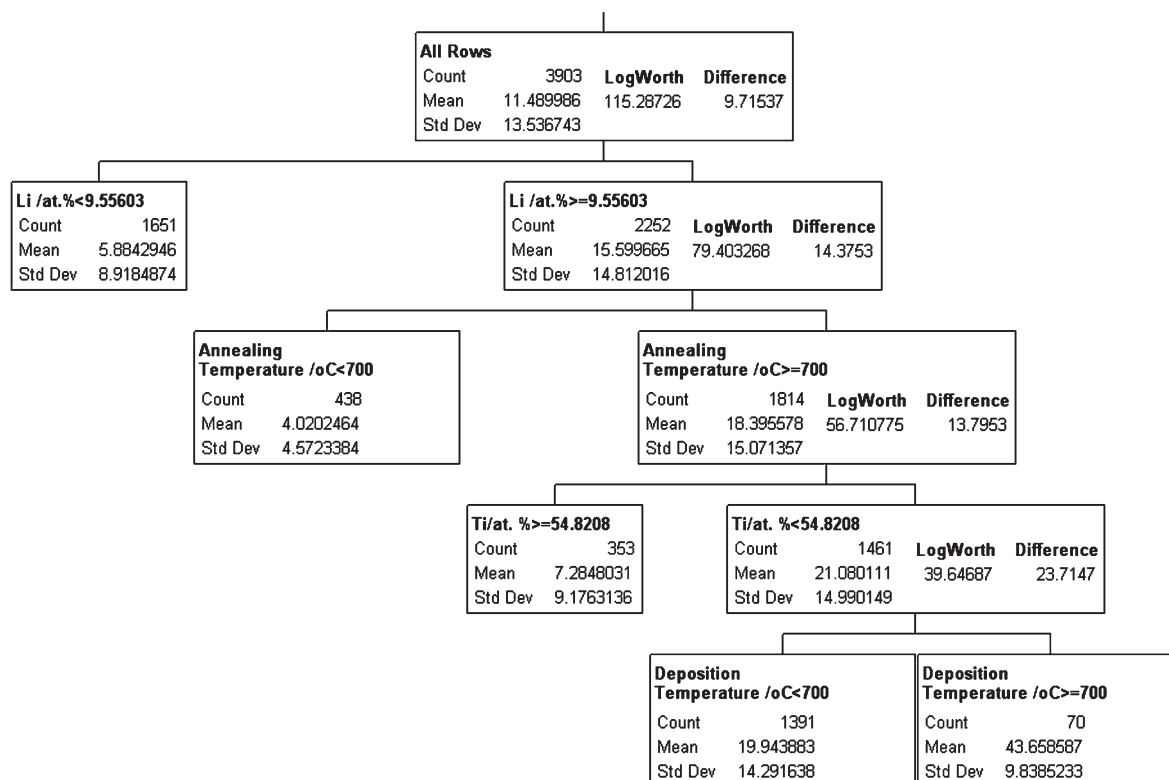


Figure 6. Recursive partitioning analysis of the effect of synthetic parameters (elemental composition, thickness, deposition, and annealing temperatures) on the percentage $\text{Li}_{3x}\text{La}_{2/3-x}\text{TiO}_3$ observed within the samples deposited on SSTOP.

The second most important factor in achieving high concentrations is the annealing temperature.

To make best use of the large number of data points collected, over a wide range of parameter space (composition, thickness, deposition temperature, annealing temperature) an artificial neural network was constructed utilizing 11 selected samples from the data set of 35. Sample libraries were selected from sets deposited on SSTOP and SSTP based on compositional range covered, range of thermal parameters, and the number of fields exhibiting capacitive behavior. To ensure a reliable set of conductivity measurements, the results from the automated analysis were verified by hand.

Description of Neural Network Modeling. A radial basis neural network was utilized throughout; modeling was carried out using MATLAB (2010a, The Mathworks) including the Neural Network Toolbox (7.0, The Mathworks). This type of model was used as it is quicker to train and is more appropriate for use with smaller data sets than other network types.²⁸

The model was constructed using a Model Data Matrix (MDM), which consisted of the eight parameters that were thought to influence the ionic conductivity behavior of the material being studied. These parameters were selected based on scientific knowledge and the partition analysis performed previously. The content of the MDM was preprocessed to account for missing values, and to remove any outlying data points. Only samples which exhibited a capacitive response were considered.

It was found that the process of random data division gave rise to differing neural network responses, all with reasonable fitting parameters. Therefore, 20 iterations of the model were evaluated, each with the same parameters. The data was redivided randomly

at the start of each iteration. Over the 20 iterations calculated, the mean correlation was found to be 0.95, 0.92, 0.92 for the training, validation, and testing data sets, respectively. The correlation was not noted to be significantly reduced for 1000 iterations.

The elemental composition and phase concentration of $\text{Li}_{3x}\text{La}_{2/3-x}\text{TiO}_3$ was then used in conjunction with the neural network model to predict the total conductivity of the Li–La–Ti–O system. The mean predicted total conductivity (20 iterations) of the Li–La–Ti–O system is shown in Figure 7. Empirical data (elemental and phase composition) for samples deposited on SSTOP at 25 °C and annealed at 700 °C was used to simulate this data, assuming a thickness of 349 nm. Although the predicted value of the total conductivity was higher than that observed in the literature ($7 \times 10^{-5} \text{ S cm}^{-1}$),¹ the optimum value was observed to coincide with the maximum observed in the literature ($\text{Li}_{0.18}\text{La}_{0.28}\text{Ti}_{0.54}$ $\sigma_{\text{Total}} = 7 \times 10^{-5} \text{ S cm}^{-1}$, $x = 0.11$).¹ The mean predicted total conductivity of the solid solution line, $\text{Li}_{3x}\text{La}_{2/3-x}\text{TiO}_3$, is shown in Figure 7.

CONCLUSIONS

The use of high throughput physical vapor deposition to synthesize $\text{Li}_{3x}\text{La}_{2/3-x}\text{TiO}_3$ has proved to be successful. Although it was not possible to produce the phase pure perovskite, it was possible to determine the ionic conductivity behavior of the system utilizing an artificial neural network model. This model, based on empirical data, enabled the determination of the highest total conductivity value within the range of compositions studied, assuming deposition was carried out at 25 °C followed by annealing at 700 °C.

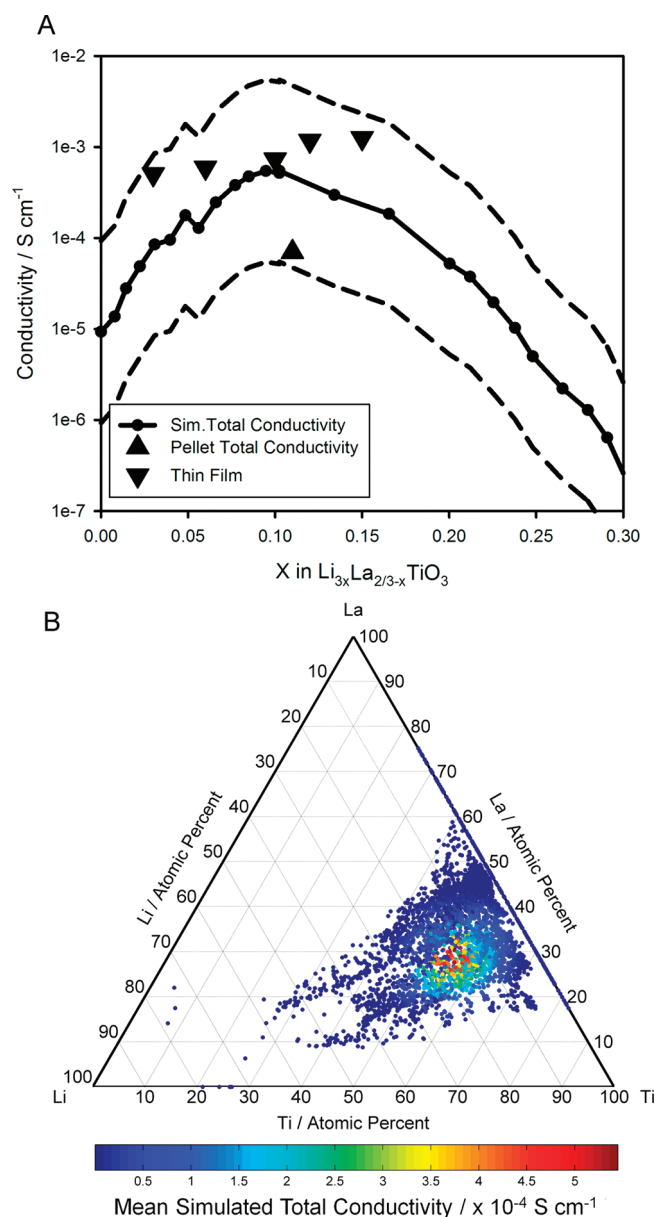


Figure 7. (A) Predicted total conductivity versus x in $\text{Li}_{3x}\text{La}_{2/3-x}\text{TiO}_3$. The solid line shows the mean simulated total conductivity (20 iterations); the variation in the simulated value is shown by the dashed lines. Total conductivities measured on pellets¹ and amorphous thin films²⁹ are shown. Although the optimum mean predicted value is higher than the observed value in the literature, within the variation of the model the two values agree. Importantly the position of the optimum value is predicted correctly ($x = 0.11$). (B) Predicted total conductivity as a function of composition. The conductivity was predicted using the artificial neural network based on empirical results. In this case the predicted conductivity is for materials deposited on SSTOP at 25 °C and annealed at 700 °C. The thickness was set to the mean value of the empirical data (349 nm). The compositions used in the prediction set (elemental and crystalline LLTO) were taken from the SSTOP empirical data set.

The synthetic method described here demonstrates significant advantages over other thin film methodologies, such as pulsed laser deposition,^{6,29} RF sputtering,³⁰ and electron beam evaporation.⁷ All of these techniques require bulk materials for each composition to be studied typically limiting studies to small

numbers of compositions. Such studies do not generally enable the experimentalist to access thermodynamically unstable materials, which are accessible via the mixing of elements at an atomic level. Since the high temperatures (1100–1200 °C) typically required to form the perovskite materials were not required during this study, the loss of lithium during processing was reduced.³¹ The use of lower temperatures has also reduced the decomposition and disproportionation of the materials. The same limitations are also encountered in bulk synthesis. A true optimization of a material system is therefore not viable, unless the problem is tackled in a high throughput manner, such as that described here.

By applying data analysis techniques usually used in data mining, such as partition analysis, it has been possible to determine the important parameters to synthesize successful $\text{Li}_{3x}\text{La}_{2/3-x}\text{TiO}_3$ thin films for analysis by electrochemical impedance spectroscopy. In this case the choice of substrate proves to be important, with SSTOP, Si/Pt, and SSTOP/SRO exhibiting greater number of capacitive measurements. Additionally, this analysis has indicated that the composition, specifically the lithium content, and the annealing temperatures are the important factors when producing a crystalline $\text{Li}_{3x}\text{La}_{2/3-x}\text{TiO}_3$ film on SSTOP.

Empirical observations, as well as partition analysis, also indicate thickness may be of importance. In the case of thin films, two hypotheses are put forward. The thinner films exhibit pin holes or cracking, leading to short circuits after the deposition of the Pt electrodes.²⁹ Alternatively, the thin films may be pierced during the measuring process, leading to direct contact between the probe and the Pt electrode.

Analysis of raw diffraction data by Principal Component Analysis (PCA) and Multivariate Curve Resolution-Alternative Least Squares (MCR) allowed phase distribution diagrams to be produced in the case of fields deposited on SSTOP and MgO.

■ ASSOCIATED CONTENT

S Supporting Information. Complete experimental details, including details of the instruments used are provided. Details of the threshold values used to classify each impedance response are given, along with an example set of impedance data, including behaviors at elevated temperature. Preprocessing details are provided for XRD data, further details of the neural network data set are also provided. The results of the partition analysis of the entire data set using the electrical classification as the responses are provided. Additional compositional maps of Groups A and B, determined from this analysis, are also shown. A comparison of the PCA and MCR fits is shown as a means to determine the number of components required to successfully model the diffraction data. Fractional distribution of components, used to generate the phase distribution diagrams shown in Figures 3 and 5 are provided for the readers interest. This material is available free of charge via the Internet at <http://pubs.acs.org>.

■ AUTHOR INFORMATION

Corresponding Author

*E-mail: beh@soton.ac.uk.

Funding Sources

The authors would like to acknowledge the funding of this work by Toyota Motor Corporation.

Notes

No conflicts of interest are declared by the authors.

ACKNOWLEDGMENT

Thanks to Professor Derek C. Sinclair for aiding the authors in the interpretation of the impedance data.

ABBREVIATIONS

PCA Principal Component Analysis
MCR Multivariate Curve Resolution
HT-PVD High Throughput Physical Vapor Deposition

REFERENCES

- (1) Inaguma, Y.; Liqian, C.; Itoh, M.; Nakamura, T.; Uchida, T.; Ikuta, H.; Wakihara, M. High Ionic Conductivity in Lithium Lanthanum Titanate. *Solid State Commun.* **1993**, *86* (10), 689–693.
- (2) Kawai, H.; Kuwano, J. Lithium Ion Conductivity of A-Site Deficient Perovskite Solid Solution $\text{La}_{0.67-x}\text{Li}_{3x}\text{TiO}_3$. *J. Electrochem. Soc.* **1994**, *141* (7), L78–79.
- (3) Kitaoka, K.; Kozuka, H.; Hashimoto, T.; Yoko, T. Preparation of $\text{La}_{0.5}\text{Li}_{0.5}\text{TiO}_3$ perovskite thin films by the sol-gel method. *J. Mater. Sci.* **1997**, *32*, 2063–2070.
- (4) Maqueda, O.; Sauvage, F.; Laffont, L.; Martínez-Sarrión, M. L.; Mestres, L.; Baudrin, E. Structural, microstructural and transport properties study of lanthanum lithium titanium perovskite thin films grown by Pulsed Laser Deposition. *Thin Solid Films* **2008**, *516*, 1651–1655.
- (5) Morcrette, M.; Gutierrez-Llorente, A.; Laurent, A.; Perrière, J.; Barboux, P.; Boilot, J. P.; Raymond, O.; Brousse, T. Growth by laser ablation of Ti-based oxide films with different valency states. *Appl. Phys. A: Mater. Sci. Process.* **1998**, *67*, 425–428.
- (6) Ahn, J.-K.; Yoon, S.-G. Characteristics of perovskite ($\text{Li}_{0.5}\text{La}_{0.5}$) TiO_3 solid electrolyte thin films grown by pulsed laser deposition for rechargeable lithium microbattery. *Electrochim. Acta* **2004**, *50*, 371–374.
- (7) Li, C.-L.; Zhang, B.; Fu, Z.-W. Physical and electrochemical characterization of amorphous lithium lanthanum titanate solid electrolyte thin-film fabricated by e-beam evaporation. *Thin Solid Films* **2006**, *515*, 1886–1892.
- (8) Dudney, N. J., Glass and Ceramic Electrolytes for Lithium and Lithium-Ion Batteries. In *Lithium Batteries Science and Technology*; Nazri, G.-A., Pistoia, G., Eds.; Springer: New York, 2009; pp 623–642.
- (9) Guerin, S.; Hayden, B. E. Physical Vapor Deposition Method for the High-Throughput Synthesis of Solid-State Material Libraries. *J. Comb. Chem.* **2006**, *8*, 66–73.
- (10) Guerin, S.; Hayden, B. E. Vapour Deposition Method. Patent EP1670966 21-06-2006, 2006.
- (11) Guerin, S.; Hayden, B. E.; Lee, C. E.; Mormiche, C.; Russell, A. E. High-throughput synthesis and screening of ternary metal alloys for electrocatalysis. *J. Phys. Chem. B* **2006**, *110* (29), 14355–14362.
- (12) Guerin, S.; Hayden, B. E.; Pletcher, D.; Rendall, M. E.; Suchsland, J. P. A combinatorial approach to the study of particle size effects on supported electrocatalysts: Oxygen reduction on gold. *J. Comb. Chem.* **2006**, *8* (5), 679–686.
- (13) Guerin, S.; Hayden, B. E.; Smith, D. C. A. High-throughput Synthesis and Screening of Hydrogen-Storage Alloys. *J. Comb. Chem.* **2008**, *10*, 37–43.
- (14) Anderson, P. S.; Guerin, S.; Hayden, B. E.; Khan, M. A.; Bell, A. J.; Han, Y.; Pasha, M.; Whittle, K. R.; Reaney, I. M. Synthesis of the ferroelectric solid solution, $\text{Pb}(\text{Zr}_{1-x}\text{Ti}_x)\text{O}_{-3}$ on a single substrate using a modified molecular beam epitaxy technique. *Appl. Phys. Lett.* **2007**, *90*, 20.
- (15) Wang, J. S.; Yoo, Y.; Gao, C.; Takeuchi, I.; Sun, X. D.; Chang, H. Y.; Xiang, X. D.; Schultz, P. G. Identification of a Blue Photoluminescent Composite Material from a Combinatorial Library. *Science* **1998**, *279* (5357), 1712–1714.
- (16) Xiang, X. D.; Sun, X. D.; Briceno, G.; Lou, Y. L.; Wang, K. A.; Chang, H. Y.; Wallace-Freedman, W. G.; Chen, S. W.; Schultz, P. G. A Combinatorial Approach to Materials Discovery. *Science* **1995**, *268* (5218), 1738–1740.
- (17) Chang, H.; Gao, C.; Takeuchi, I.; Yoo, Y.; Wang, J.; Schultz, P. G.; Xiang, X. D.; Sharma, R. P.; Downes, M.; Venkatesan, T. Combinatorial synthesis and evaluation of epitaxial ferroelectric device libraries. *Appl. Phys. Lett.* **1998**, *72*, 2185–2187.
- (18) Briceno, G.; Chang, H.; Sun, X. D.; Schultz, P. G.; Xiang, X. D. A Class of Cobalt Oxide Magnetoresistance Materials Discovered with Combinatorial Synthesis. *Science* **1995**, *270*, 273–275.
- (19) Tsui, F.; Ryan, P. A. Combinatorial molecular beam epitaxy synthesis and characterization of magnetic alloys. *Appl. Surf. Sci.* **2002**, *189*, 333–338.
- (20) Matsumoto, Y.; Murakami, M.; Jin, Z. W.; Ohtomo, A.; Lippmaa, M.; Kawasaki, M.; Koinuma, H. Combinatorial Laser Molecular Beam Epitaxy (MBE) Growth of Mg–Zn–O Alloy for Band Gap Engineering. *Jpn. J. Appl. Phys., Part 2* **1999**, *38*, L603–L605.
- (21) Hanak, J. J. The “multiple-sample concept” in materials research: Synthesis, compositional analysis and testing of entire multi-component systems. *J. Mater. Sci.* **1970**, *5* (11), 964–971.
- (22) Koinuma, H. Quantum functional oxides and combinatorial chemistry. *Solid State Ionics* **1998**, *108* (1–4), 1–7.
- (23) Stramare, S.; Thangadurai, V.; Weppner, W. Lithium Lanthanum Titanates: A Review. *Chem. Mater.* **2003**, *15*, 3974–3990.
- (24) Irvine, J. T. S.; Sinclair, D. C.; West, A. R. Electroceramics: Characterisation by Impedance Spectroscopy. *Adv. Mater.* **1990**, *2*, 132.
- (25) West, A. R.; Sinclair, D. C.; Hirose, N. Characterization of Electrical Materials, Especially Ferroelectrics, by Impedance Spectroscopy. *J. Electroceram.* **1997**, *1* (1), 65.
- (26) Long, C. J.; Bunker, D.; Li, X.; Karen, V. L.; Takeuchi, I. Rapid identification of structural phases in combinatorial thin-film libraries using X-ray diffraction and non-negative matrix factorization. *Rev. Sci. Instrum.* **2009**, *80* (10), 103902–6.
- (27) Jaumot, J.; Gargallo, R.; de Juan, A.; Tauler, R. A graphical user-friendly interface for MCR-ALS: a new tool for multivariate curve resolution in MATLAB. *Chemom. Intell. Lab. Syst.* **2005**, *76* (1), 101–110.
- (28) Tetteh, J.; Metcalfe, E.; Howells, S. *Chemom. Intell. Lab. Syst.* **1998**, *41*, 17–29.
- (29) Furusawa, S.; Tabuchi, H.; Sugiyama, T.; Tao, S.; Irvine, J. T. S. Ionic conductivity of amorphous lithium lanthanum titanate thin film. *Solid State Ionics* **2005**, *176*, 553–558.
- (30) Morales, M.; Laffez, P.; Chateigner, D.; Vickridge, I. Characterisation of Lanthanum Lithium Titanate Thin Films Deposited by radio frequency sputtering on [100] oriented MgO substrates. *Thin Solid Films* **2002**, *418*, 119–128.
- (31) Tatsumisago, M.; Hayashi, A. Preparation of lithium ion conducting glasses and glass-ceramics for all-solid-state batteries. *J. Non-Cryst. Solids* **2008**, *354*, 1411–1417.

NOTE ADDED AFTER ASAP PUBLICATION

This paper was published on the Web on April 11, 2011, with an error in the affiliation and Funding Statement. The corrected version was reposted on May 23, 2011.